

Characterizing the Pressure Gain of Magazines due to Convective Combustion of M1 Gun Propellant

Brian T. Bojko; Naval Air Warfare Center Weapons Division; China Lake, CA, USA
Nathaniel Davis; Naval Air Warfare Center Weapons Division; China Lake, CA, USA
Cynthia Romo; Naval Air Warfare Center Weapons Division; China Lake, CA, USA
Ephraim Washburn; Naval Air Warfare Center Weapons Division; China Lake, CA, USA
Alice I. Atwood; Naval Systems Integrated; Ridgecrest, CA, USA
Josephine Covino; Department of Defense Explosives Safety Board; Alexandria, VA, USA

Keywords: Convective Combustion, CFD, Modeling, H1.3, M1, Pressurization

Abstract

Experimental results of the deflagration of *M1* gun propellant, an HD1.3 material, are used to develop a burning-rate versus pressure model to be used in large scale simulations. The burning-rate model of the *M1* is used as the boundary condition for a propellant within a magazine after it has been ignited. To validate the approach and determine the effects of combustion temperature on magazine pressurization, detailed two-dimensional simulations are conducted and compared to the small-scale experiments. The pressure gain in the simulations were within 5% of the experimental data for combustion temperatures of 2800 – 3000K. After validation of the model at small scales, a three-dimensional large-scale combustion simulation of a vented magazine was conducted for varying loading densities and venting areas. Results are presented showing the effects of Mach number and internal pressure as a function of the vent-area-ratio at different loading densities.

Introduction

Safe storage of energetic material is currently determined by a safety distance function that is proportional to the weight of the hazardous material. However, weight-based methods are insufficient in determining safe distances when HD1.3 systems ignite and deflagrate within a structure, increasing the internal pressure and inducing choked flow at the exit resulting in violent ejections of energetic materials. To increase the safety of such systems, it is critical to explore the loading densities and venting areas of the storage facilities to evaluate risks of propellant deflagration.

The rest of this study is organized as follows. First, a brief description of the experimental setup that was used to develop and validate the numerical models is presented. Then, the mathematical formulation of the burning-rate versus pressure model is developed from the small-scale experimental data. The multi-dimensional, compressible Navier-Stokes equations with Large Eddy Simulations (LES) to account for combustion and turbulence effects is presented. This model is used for both the *2D* and *3D* detailed and large-scale combustion simulations, respectively. Results of a two-dimensional detailed simulation of the combustion of *M1* propellant in a poly-carbonate tube are presented for different combustion temperatures and compared to experimental data for model validation. The burning-rate model and combustion temperature are then combined and used to simulate a large-scale magazine structure at varying loading densities (LD) and vent-area-ratios (VAR). Simulation results of the magazine structure are presented and discussion on effects of LD and VAR are presented. Conclusions are drawn regarding the burning-rate model and its validation in the *2D* simulations, along with the results of the large-scale *3D* simulations. Finally, Appendix A offers an example of the collaboration between experimentalists and modelers, and how the two approaches can compliment one another to answer important scientific questions.

Experimental Background

Figure 1 shows a schematic of the experimental setup used in this study to determine the burning-rate versus pressure at small scales. The schematic shows a poly-carbonate tube sandwiched between two steel plates (not shown) with a pressure gauge on the top and bottom of the chamber. The M1 propellant is sprinkled into the tube without additional packing to a bed height (F) around 8.25in for each run. The igniter, which is a Red Dot smokeless powder, was calibrated to provide just enough energy to the propellant bed to achieve ignition and self-propagation. A high-speed camera is trained on the polycarbonate tube containing the M1 propellant and igniter to obtain a burning-rate in time. The experimental results provide a burning-rate of the propellant as a function of the chamber pressure and will be used to develop the model discussed in Section 3.

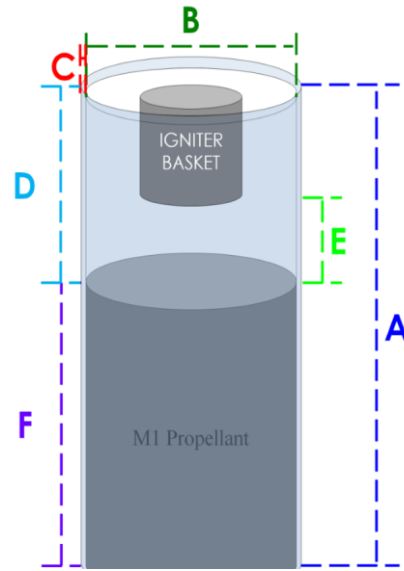


Figure 1: Illustration of the experimental configuration used in this study.

Mathematical Formulation

Burning-rate versus Pressure

The first step in developing a realizable deflagration combustion simulation for large scales, is to create a burning-rate versus pressure model that can be used to describe the coupling of ambient conditions to the pyrolysis and combustion of the gun propellant. To develop this model, an empirical relation of the M1 burning-rate and chamber pressurization was taken from small-scale experiments of M1 propellant burning in a polycarbonate tube. The chamber is equipped with a pressure tap at the top and bottom of the tube and is imaged with a high-speed camera. The data for the burning-rate and fits are provided by Romo *et al.* [1] and are shown in Fig. 2. Figure 2(a) shows the raw data of the burning M1 in time and Fig. 2(b) are the empirical curve fits used in this study.

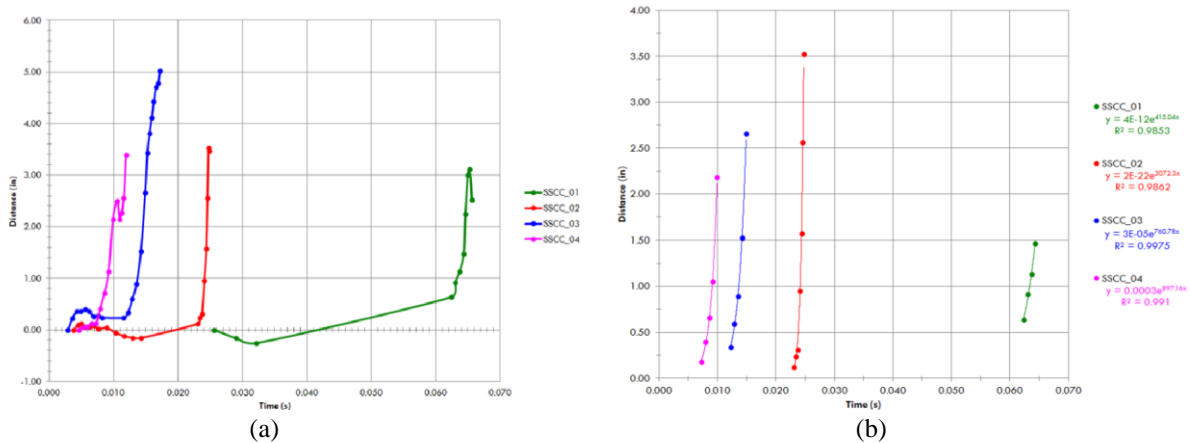


Figure 2: Experimental burning-rates of 4 combustion tests showing the (a) raw data and (b) the empirical curve fits used to create the burning-rate model.

The raw data from the top pressure sensor is fit to an exponential function given as, $P = b * e^{(a*t)}$. Figure 3 shows the raw data for the top pressure gauge for four different experimental runs labeled as, “SSCC 0X”, where X ranges between 1 and 4. Each number in the plots corresponds to a specific event or pressure rise during the runs. The pressure curve fit was taken between points 4 and 5 for each dataset, as this is the point that corresponds to the deflagration of the M1 propellant. The only exception being the SSCC 04 case where the major event is located between points 3 and 4. The root-mean-square (R^2) of each curve fit was, 0.926, 0.947, 0.907, and 0.989 for each run, SSCC 01, SSCC 02, SSCC 03, and SSCC 04, respectively.

The final process in obtaining the burning-rate versus pressure in units of, kg/s vs. Pa , is to convert the experiment values from in/s using the loading densities and psi to Pa . The loading density for each run ranged from $884.1kg/m^3$ to $905.7kg/m^3$ with an average value of $896.8kg/m^3$ and corresponds to a “hand-sprinkled” approach, where propellant is poured into the container without additional packing. The relationship between the burning-rate and pressure was assumed to have a relationship of, $r_b = b * P^n$, where r_b is the burning-rate, b is the scalar coefficient, P is the pressure, and n is the exponential coefficient. This is a similar approach to solid propellant burning-rate correlations. The values of b and n are determined using all four runs, except for SSCC 02, which has been excluded due to the exponential coefficient for this case being twice as large as all other cases. The values of b and n are determined to be $2.897e - 08$ and 1.939 respectively. Figure 4 shows the fits of burning-rate vs. pressure for the three experimental cases, SSCC 01, SSCC 03, and SSCC 04, along with the average line for the three ones that will be used in the model.

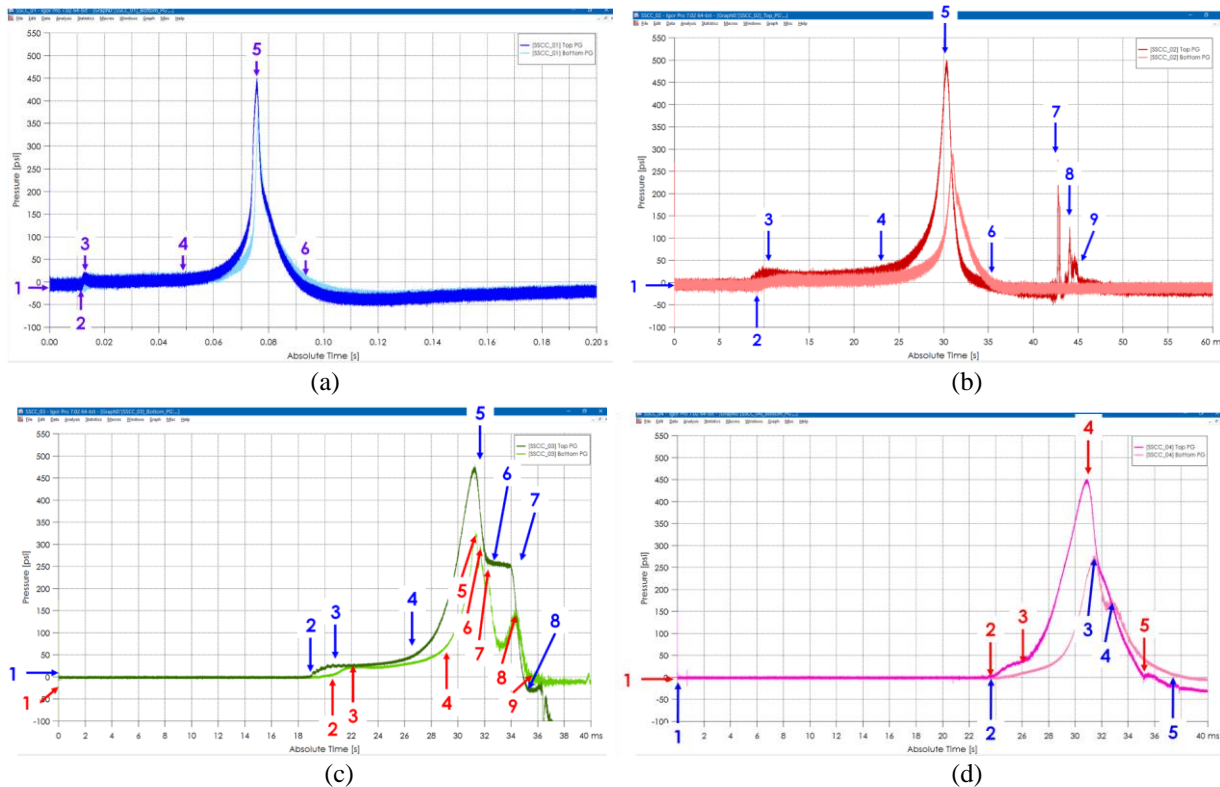


Figure 3: Experimental pressure tap results at the top pressure gauge for four different runs labeled, (a) SSCC 01, (b) SSCC 02, (c) SSCC 03, and (d) SSCC 04.

Combustion Model

The computational fluid dynamics (CFD) modeling methodology is based on the use of large eddy simulations (LES) where the Navier-Stokes equations are pre-filtered using a positive definite filtering function, G , (i. e., $G(\Delta_f, |\mathbf{x} - \mathbf{x}'|) > 0 \forall \mathbf{x}'$) possessing the usual normalization and symmetry properties, where Δ_f is the filter width. A Favre filtered quantity, $\tilde{\phi}$, is defined by the following convolution integral.

$$\tilde{\phi}(\mathbf{x}) = \frac{\overline{\rho\phi}}{\bar{\rho}} = \frac{1}{\bar{\rho}} \int_D \rho(\mathbf{x}') \phi(\mathbf{x}') G(\Delta_f, |\mathbf{x} - \mathbf{x}'|) d\mathbf{x}' \quad (1)$$

Application of the filtering to the compressible form of the Navier-Stokes equations results in the following set of model transport equations for mass, momentum and energy,

$$\frac{\partial \bar{\rho}}{\partial t} + \nabla \cdot (\bar{\rho} \tilde{\mathbf{u}}) = 0 \quad (2a)$$

$$\frac{\partial (\bar{\rho} \tilde{\mathbf{u}})}{\partial t} + \nabla \cdot (\bar{\rho} \tilde{\mathbf{u}} \tilde{\mathbf{u}}) = \nabla \cdot (-\bar{p} \tilde{\mathbf{I}} + \tilde{\boldsymbol{\tau}} + \tilde{\mathbf{T}}_{uu}) + \bar{\rho} \tilde{\mathbf{g}} \quad (2b)$$

$$\frac{\partial (\bar{\rho} \tilde{e}_t)}{\partial t} + \nabla \cdot (\bar{\rho} \tilde{\mathbf{u}} \tilde{h}_t) = \nabla \cdot (\tilde{\mathbf{T}}_{uh_t} + \tilde{\mathbf{u}} \cdot \tilde{\boldsymbol{\tau}} - \bar{\mathbf{q}}) + \bar{\rho} \tilde{\mathbf{u}} \cdot \tilde{\mathbf{g}} \quad (2c)$$

where $\bar{\rho}$ is the density, $\tilde{\mathbf{u}}$ is the velocity, \bar{p} is the pressure, $\tilde{e}_t (= \tilde{h}_t - \tilde{R}\tilde{T})$ is the total resolved energy and $\tilde{h}_t (= \tilde{h} + \tilde{\mathbf{u}} \cdot \tilde{\mathbf{u}}/2)$ is the total enthalpy including the resolved sensible enthalpy (\tilde{h}) and kinetic energy. A compressible Newtonian fluid is assumed for the viscous stress tensor, $\tilde{\boldsymbol{\tau}} = -\frac{2}{3} \mu(\tilde{T}) \tilde{\mathbf{I}} \nabla \cdot \tilde{\mathbf{u}} + \mu(\tilde{T}) (\nabla \tilde{\mathbf{u}} + (\nabla \tilde{\mathbf{u}})^T)$. Equal diffusivities are assumed for all species and radiation heat transfer is ignored thereby simplifying the heat flux, $\bar{\mathbf{q}} = -\mu(\tilde{T}) \left[\frac{c_p}{Pr} \left(1 - \frac{1}{Le} \right) \nabla \tilde{T} + \frac{1}{Sc} \nabla \tilde{h} \right]$. The second-order correlation quantities, $\tilde{\mathbf{T}}_{\alpha\beta}$, in Eqs. (2b) through (2c) represent unknown subgrid-scale (SGS) correlation for variables α and β , and are defined as: $\tilde{\mathbf{T}}_{\alpha\beta} \equiv -\bar{\rho}(\tilde{\alpha}\tilde{\beta} - \tilde{\alpha}\tilde{\beta})$. An abundance of models are currently available for closing these terms. The most common SGS models are the dynamic Smagorinsky and gradient diffusion models which are the ones used in this study [2]. Since the focus of this study isn't on LES SGS models, the interested reader is referred to [3, 4] for additional details.

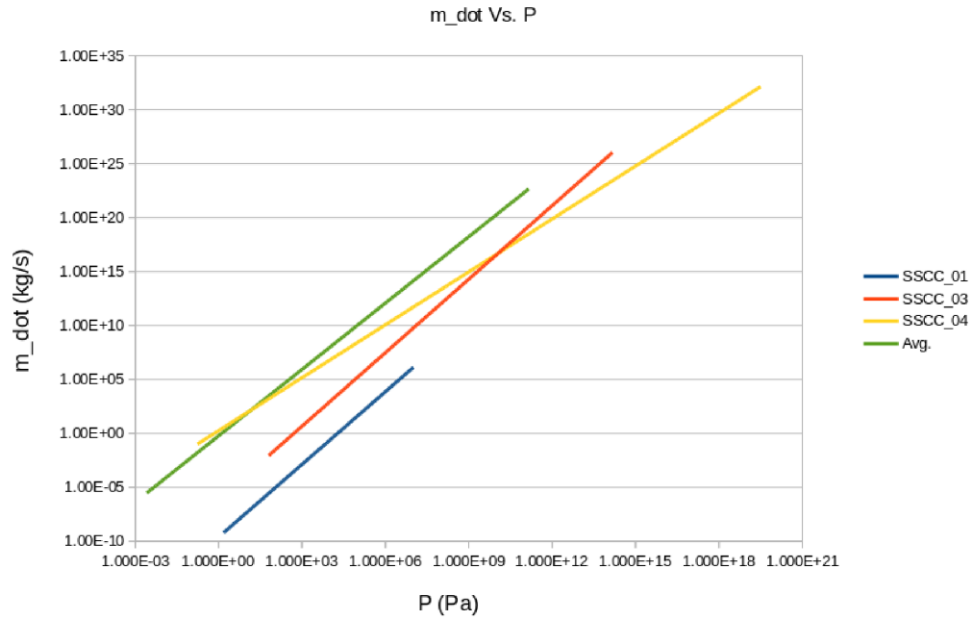


Figure 4: Empirical fit for the burning-rate (kg/s) versus the chamber pressure (Pa).

The use of LES was desirable to resolve the turbulent combustion occurring within the magazine chamber while still maintaining computational efficiency by modeling the turbulence on the smallest scales. A finite volume method is used to solve the coupled system of non-linear equations and second-order fractional step method is used to integrate the equations using a two-stage Runge-Kutta time integration. Convective fluxes are discretized using an AUSM+UP flux vector splitting [5] with a combination of second-order upwind biased and essentially non-oscillatory (ENO) interpolants for determining fluxes [6, 7]. Molecular fluxes are approximated using second-order centered differencing employing a semi-implicit operator to avoid diffusion time step stability limitations. This approach is used for the two-dimensional simulations of the small-scale experiment and the large-scale simulations of a $2m \times 2m \times 2m$ magazine at different loading densities.

Results and Discussion

2D Combustion

Two-dimensional simulations of the experimental setup shown in Fig. 2 are conducted through the axis of symmetry. The poly-carbonate tube is modeled as an adiabatic wall due to the fast time scales of the deflagration wave compared to the thermal mass of the container. The remaining boundary is modeled as the burning propellant with a constant combustion temperature (to be determined) and the burning-rate vs. pressure model sets the mass flow rate at the surface. In this particular case, a combustion temperature of the *M1* propellant could be chosen based on the heat of combustion etc., but because an empirical fit to the burning-rate is considered, the combustion temperature is chosen such that the 2D simulations match the experimental data. Starting from 800K and moving up to a combustion temperature of $T_{comb} = 3000K$, the 2D simulation is repeated and the pressure rise at the top boundary is cataloged and compared to experimental data. The initial conditions are set to ambient temperature and pressure with a small perturbation of the pressure (5%) near the propellant surface to trigger the deflagration model. The solid black boundary in Fig.5 represents the poly-carbonate tube on the left, top, and right boundaries, while the brown line at the bottom represents the *M1* propellant boundary.

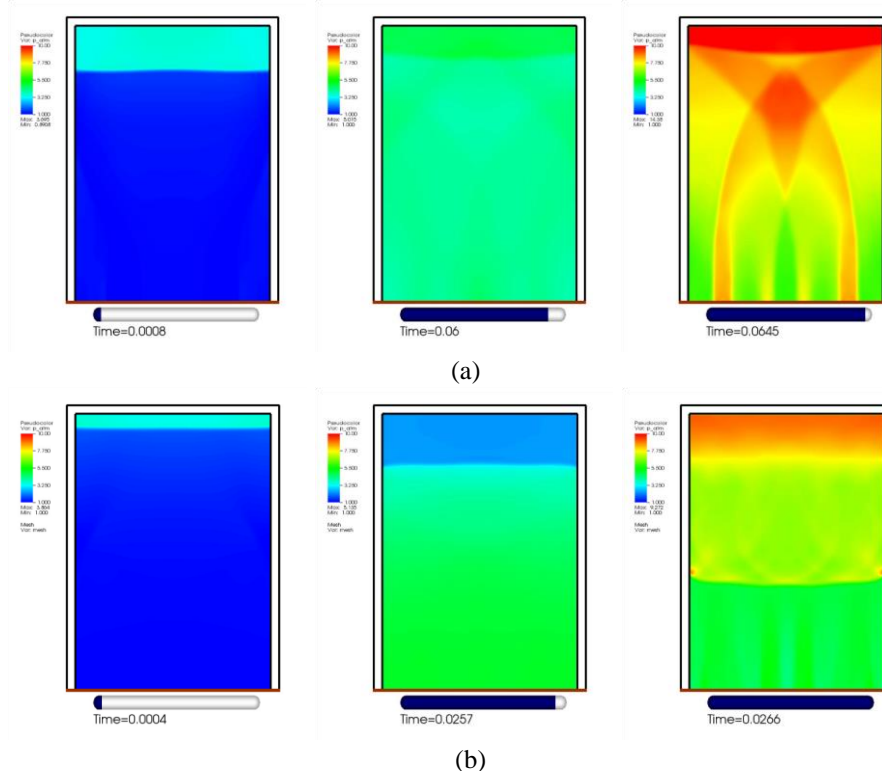


Figure 5: Two-dimensional combustion simulations of the *M1* deflagration showing the pressure gain at the lower combustion temperature (a) $T_{comb} = 800K$ and (b) $T_{comb} = 3000K$.

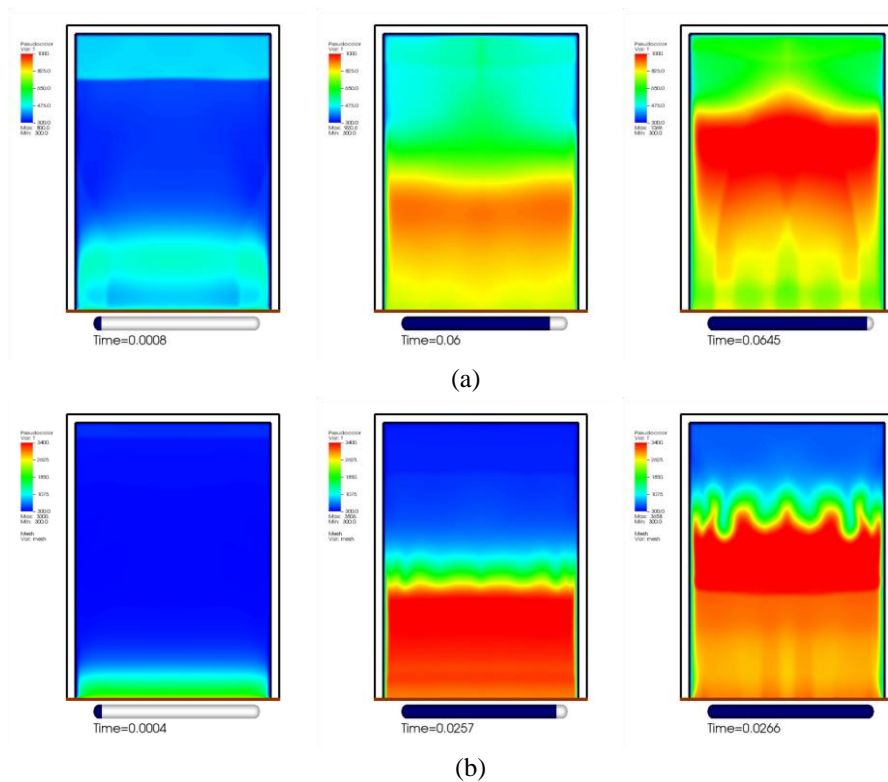


Figure 6: Two-dimensional combustion simulations of the M1 deflagration showing the temperature gain at the lower combustion temperature (a) $T_{comb} = 800K$ and (b) $T_{comb} = 3000K$.

Figure 5 shows the pressure gain of the poly-carbonate tube at three different time steps for the lowest combustion temperature (Fig.5(a)) and the highest combustion temperature (Fig.5(b)) of $T_{comb} = 800K$ and $T_{comb} = 3000K$, respectively. As can be seen from Fig. 3, the pressure gain is exponential, so the contour plot for the pressure is set from 0 to $10atm$, where structural failure occurs rapidly beyond the last image shown. Figure 5 shows how the pressure wave travels from the top of the combustion chamber back to the propellant bed, causing minute pressure oscillations as the overall pressure in the chamber continues to rise. Pressure wave interactions are evident for both cases, especially for the last time step shown. The major difference between the $T_{comb} = 800K$ and the $T_{comb} = 3000K$ cases are firstly, how quickly the chamber pressurizes. For $T_{comb} = 3000K$, the pressure gain is approximately 3 times faster than that of the $T_{comb} = 800K$ case. The second major difference is the uniformity of the pressure gain just before failure, the low combustion temperature shows a very non-uniform pressure gradient in the radial direction, while the higher combustion temperature appears more uniform in the $r - dir$ and a wave front is more apparent.

Figure 6 shows the temperature gain and distribution for the low and high combustion temperatures in Fig.6(a) and Fig.6(b), respectively. The scale for the temperature contour plot is set from $T = 300 - 1000K$ for $T_{comb} = 800K$ and is set to $T = 300 - 3400K$ for the $T_{comb} = 3000K$ case. The time-stamps are kept consistent between Figs.5 and 6 for easy comparison. The temperature rise for $T_{comb} = 800K$ is more uniform, but much lower than the $T_{comb} = 3000K$ case, but is lower in magnitude by roughly 3 times. These two plots show the significance in choosing the correct combustion temperature in order to obtain the desired response observed in the experiments. The lower combustion temperature shows a much slower response and lower temperature gains than the higher combustion temperature, both of which are approximately 3 times larger for $T_{comb} = 3000K$ than $T_{comb} = 800K$.

Figure 7 shows the pressure gain versus time for nine different combustion temperatures (lines) ranging from $T_{comb} = 800 - 3000K$ compared to the pressure gain of the top gauge during the experimental runs (symbols). The three lowest temperatures are colored in blue, then the middle range is colored red, followed by the highest two combustion temperatures shown in black. The pressure gain of the lowest temperatures show a very slow time response with a gradual increase in the chamber pressure. The next set of temperatures (red lines) show more

promise in increasing the chamber pressure, but are also much too gradual to capture the large spike in pressure seen in the experimental data. The lower temperatures show an over-predicted pressure gain in the early time frame, but then soon drastically under-predict pressure gain. Finally, $T_{comb} = 2800K - 3000K$ follows the experimental data well in both magnitude and response time with errors to the experimental data no greater than 20%. The sharp transition in pressure near $t = 0.024s$ is captured well by the higher combustion temperatures. Moving forward, the combustion temperature of the three-dimensional cases will be set to $T_{comb} = 2800K$. This now provides the two boundary conditions necessary at the deflagrating propellant surface to account for the burning-rate as a function of pressure and the combustion temperature.

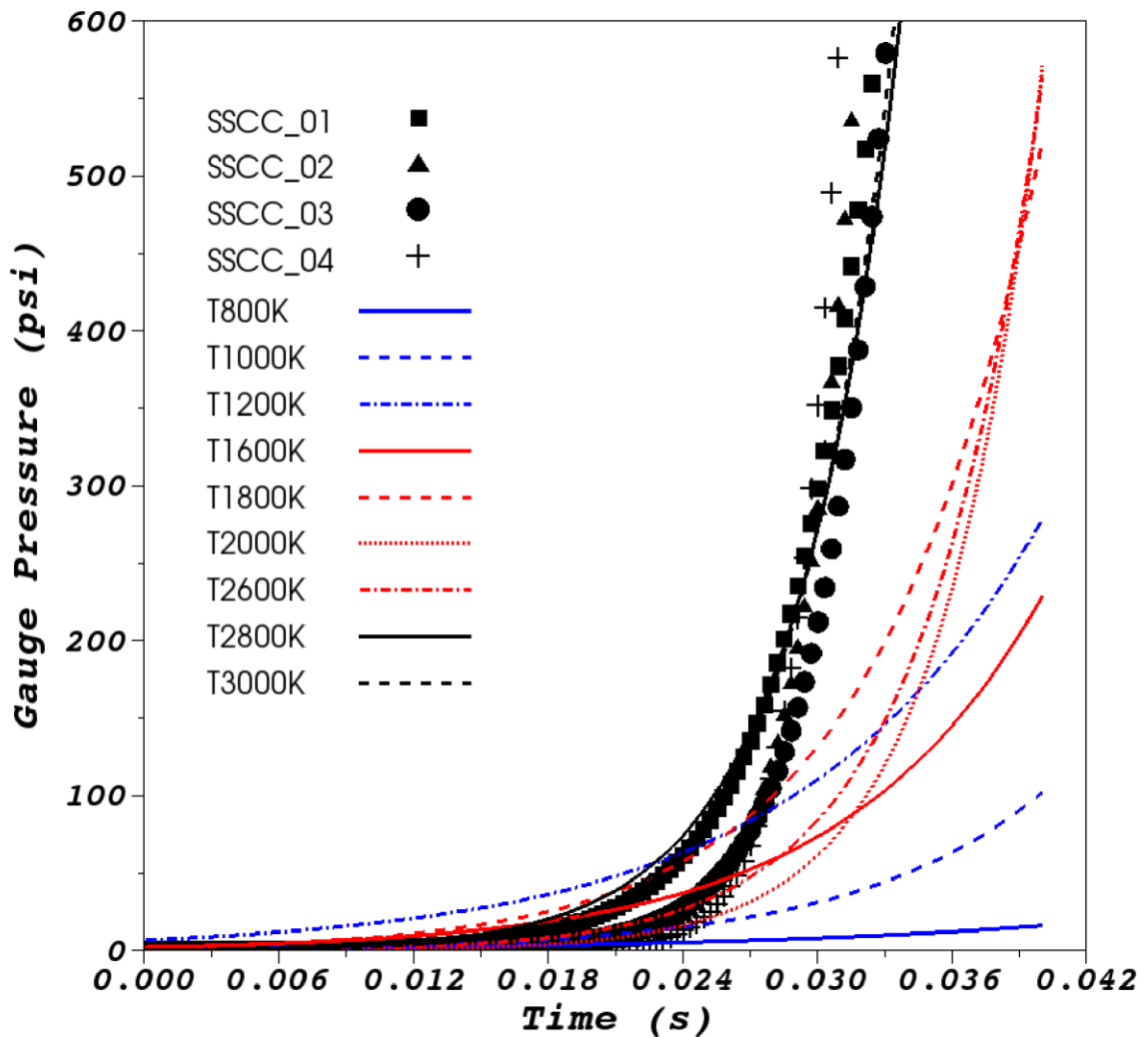


Figure 7: Pressure gain of the poly-carbonate tube at different combustion temperatures ranging from 800 – 3000K (lines) compared to the experimental data (symbols).

3D Combustion

The large scale combustion simulations conducted in this study are modeled after the experimental, $2m \times 2m \times 2m$, Kasun structure which is used as a make-shift magazine for $M1$ gun propellant as presented in Ref.[8]. The Kasun structure is an $8m^3$ concrete structure with $15.2cm$ ($6in$) walls and housed burning $M1$ gun propellant at a loading density of 15 and $63kg/m^3$. Four experiments were carried out at the two different loading densities with a venting diameter in the front of the structure that was $79cm$ and $39cm$ for the low and high loading densities,

respectively. A variation in the perforations of the propellant from 1P (a single perforation) to 7P (seven perforations) were considered between the different setups. Figure 8 shows the solid models of the smaller diameter (39cm) and the larger diameter (79cm) used to vent the hot gases during combustion.

The CFD simulations use the same flow solver described previously and include LES for turbulence modeling. A computational grid is constructed to include the entire Kasun structure and 3m in front of the structure. To resolve small flow features, the grid consists of 5.2 million grid points, with a resolution of 1.7cm per node. Three-dimensional CAD models of the structure are exported in a stereolithography format (STL) and are read into the CFD solver to model the solid boundaries of the walls. All other boundary conditions to the simulation are set to an open configuration, except for the ground which is also modeled as a solid isothermal boundary. This setup was used to conduct 14 simulations at loading densities of 15 and 63kg/m³ with varying venting diameters or vent-area-ratios (VAR), where $VAR = (\pi(D/2)^2)/(V^{2/3})$, D is the vent diameter, and V is the volume of the structure. The venting diameters were varied from $D = 9, 29, 39, 59, 69, 79,$ and 99cm for each loading density to determine how the VAR effects the pressurization and ejection of hot combustion products.

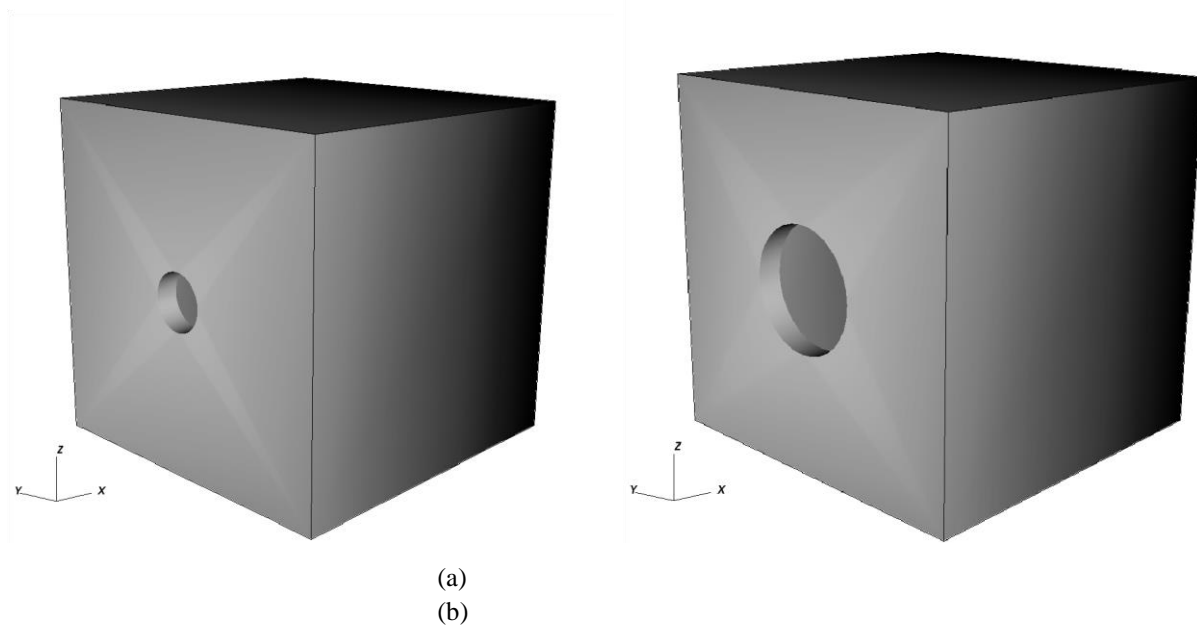


Figure 8: Solid models of the Kasun structures with the (a) 39cm and (b) 79cm venting diameter in the front of the structure.

Burning M1 propellant in the combustion simulations is an incredibly transient process involving oscillating pressure waves that affect the overall load on the magazine walls, the ejection of the hot combustion gases, and the burning rate of the propellant. Figure 9 shows three time-steps progressing from left to right for the lower loading density (15kg/m³) and the high loading density (63kg/m³) with venting diameters of $D = 9cm$ and $D = 99cm$, respectively. The Kasun structure is outlined by the edges of its walls but, made transparent for easy visibility. The drums are shown as solid black cylinders. The temperature of the domain is shown on the color mapping slices that cut through the $x, y,$ and z directions at the center of the structure. The red contour represents the flow at a Mach number of $Ma = 1$ and helps identify whether the flow becomes choked. From Fig.9(a) it is clear the flow is choked in the beginning of the simulation and sputters while the inside of the chamber is heating up and pressurizing. Figure9(b) shows a choked flow condition for the high loading density even though the diameter of the vent was increased from $D = 39cm$ in the experimental setup to $D = 99cm$ in the simulation.

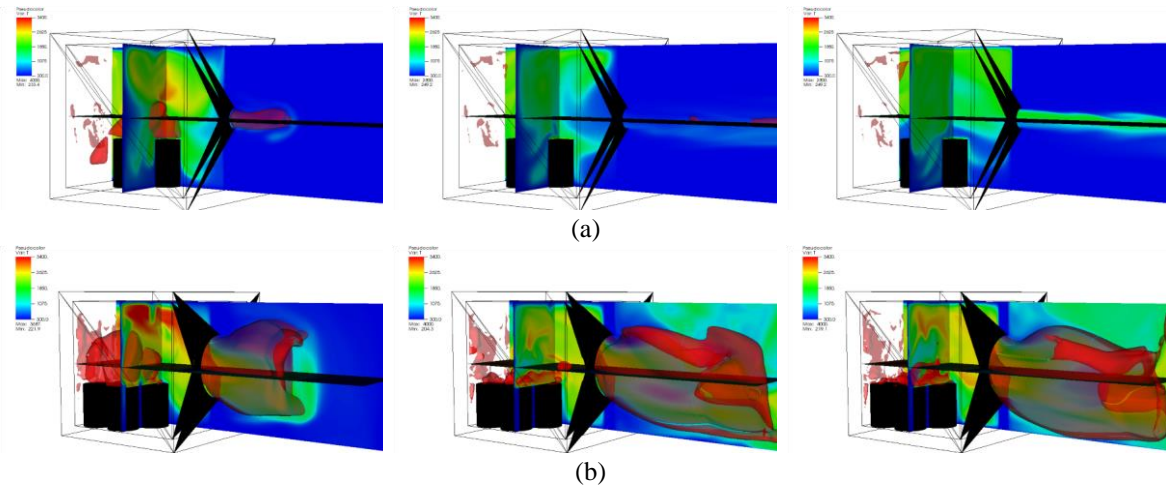


Figure 9: Three-dimensional combustion simulations of the (a) lower loading density with vent diameter of $D = 9cm$ and (b) higher loading density with vent diameter of $D = 99cm$ at three different time-steps progressing from left to right.

Comparing the low loading density with vent diameter of $D = 79cm$ and the high loading density with vent diameter of $D = 39cm$ to the experimental data of Test#3 and Test#4 from Ref.[8] offers some insight into the application of small scale burning rate models to large scale simulations. The average temperature of the ejected gas in the beginning of the simulation of Test#3 is $T_{exit} = 753.7K \pm 207.3K$ which is within the temperature range reported in [8] at the two thermocouples above and below the door with reported temperature peaks of $T_{top} = 959.462K$ and $T_{bot} = 914.144K$, respectively. For the higher loading case the temperature at the exit increases significantly with reported values above and below the door at $T_{top} = 1673.0K$ and $T_{bot} = 862.046K$. A similar trend was observed for the simulation with an increased temperature of the upper part of the door than below, with values of $T_{top} = 1449.92K$ and $T_{bot} = 1082.804K$ which are within 20% of the experimental values. The peak pressures observed in the simulations for the low and high loading densities at the top of the Kasun structure are $P_{top} = 3.528psi$ and $P_{top} = 29.7374psi$, respectively; compared to the experimental values of $P_{top} = 0.949453psi$ and $P_{top} = 33.8711psi$. While the choked flow scenario at the high loading density matches the data well, within 12%, the lower loading density is different by almost 300% but it still accurately predicts an unchoked flow. Differences at the lower loading densities could be attributed to the highly loaded, small scale experiment without venting that the burning rate model was derived from. However, the small scale experiment has provided a burning rate that appears to be highly applicable to the choked scenario. Improvements to future experiments could be to include a vent and span a range of loading densities to better understand the burning rate versus pressure. Overall, the simulations compared relatively well to the large scale experimental data of the Kasun structure and in the case of the low density limit, it could be considered as a conservative limit for pressurization. The simulations are used to extend the experimental study and are specifically used to determine the effects of the VAR at the two different loading densities. Figure10 shows the effects of the VAR on the Mach number at the exit and the pressurization of the structure for the two different loading densities, 15 (3 drums) and $63kg/m^3$ (8 drums). From Fig.10(a) it is clear to see the flow at the exit is always choked for the 8 drum case regardless of the VAR and it is always unchoked for the 3 drum case. Although the Ma number steadily increases for the low loading case, it does not become choked even when the venting diameter is as small as $9cm$. On the other extreme, the flow is always choked for the 8 drum case although the vent diameter is nearly $1m$. Therefore, it appears the leading factor in whether or not the flow will be choked is the loading density and not the VAR. Figure10(b) shows the peak pressure within the structure as a function of the VAR, where the 3 drum case shows a relatively constant pressurization because the flow is unchoked, the choked flow of the 8 drum cases shows a nearly steady pressurization with decreasing VAR. The two plots presented here provide insight into the effects of the VAR and loading densities. Firstly, whether or not the flow will be choked appears to be mostly dependent on the loading density of the magazine and relies very little on the VAR. Secondly, if the flow does become choked, the overall pressurization of the facility can be predicted based on the VAR and increases by 50% with a decrease in the VAR by a factor of 10.

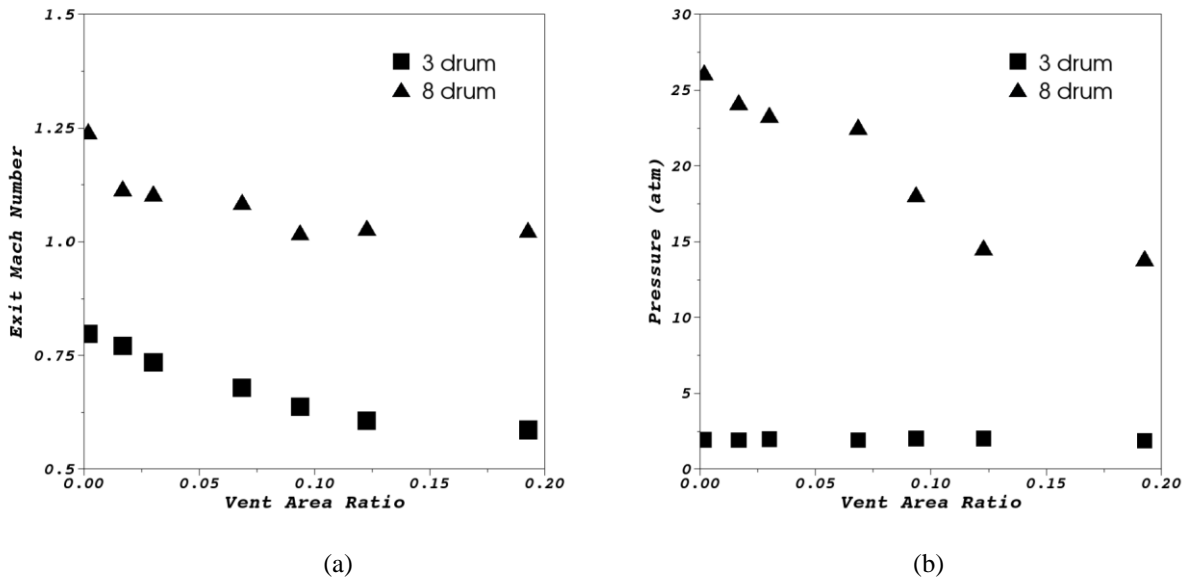


Figure 10: Simulation results of the Kasun structure at different vent-area-ratios (VAR) showing the effects on the (a) Mach number at the exit and (b) the pressurization at loading densities with 3 and 8 drums of *M1 7P* gun propellant.

Conclusion

A new model was developed for the characterization of hazardous materials in the HD1.3 classification. Specifically, the convective combustion of *M1* gun propellant was modeled in two and three-dimensions to validate the model and to computationally explore combustion scenarios that are typically costly and dangerous. The small-scale experiments of Romo and Atwood were used to calibrate a burning-rate versus pressure model in the form of, $r_b = bP^n$, where r_b is the burning-rate, P is the pressure, and b and n are the unknown coefficients. After obtaining the empirical relationship for the burning-rate as a function of pressure, it was necessary to determine the effective combustion temperature of the deflagrating *M1* and to validate the computational model before moving on to 3D simulations.

Combustion temperatures of the *M1* deflagration were chosen in a range from $T_{comb} = 800K$ to $3000K$ and were subsequently tested in a 2D simulation of the experimental setup for which the burning-rate model was obtained. The simulations of the lowest combustion temperature showed a pressure gain that was too slow to capture the pressure rise in the experimental chamber and was approximately three times slower than the response time of the chosen combustion temperature of $T_{comb} = 2800K$. With the combustion temperature at the boundary set to $T_{comb} = 2800K$, the pressure gain followed that of the experimental data with good overall agreement, and with errors no greater than 20% between all of the test cases. Upon completing the 2D simulations, there was now a burning-rate model and combustion temperature validated against experimental data, giving confidence in approach taken in this study.

After validation of the burning-rate model against the small-scale experimental setup, three-dimensional simulations were conducted based on the Kasun structure data from Ref.[8]. The pressurization and ejection temperatures of Test#3 and Test#4 were compared to the simulations and showed good overall agreement except for the pressurization values of Test#3 which were over-predicted. This is considered a conservative estimate of the overall pressurization for the unchoked flow regime. The simulations explored the effects of the vent-area-ratio (VAR) on the ejection *Ma* number and the pressurization and showed the leading order effect to determine whether the flow will be choked is the loading density. The pressurization will depend on whether the flow is choked; if it is unchoked then the pressure will be relatively constant regardless of the VAR but, if the flow is choked then the pressurization can be determined from the VAR.

A fully compressible, turbulent CFD model is developed to capture the effects of pressurization on burning-rate of *M1* propellant confined within a magazine. The burning-rate model was based on empirical data and validated against small-scale experiments to capture the overall pressurization of the container. Without a compressible formulation, which can be computationally expensive, it would be impossible to obtain accurate results of a choked flow and subsequent chamber pressurization. The ability to accurately capture the pressurization of a magazine, including the effects of burning-rate versus pressure, allows for further investigation of facility response on the large scale at a significantly reduced cost and can be supplemented through the coupling of other computational models, i.e. using finite element (FE) analysis to determine the structural response. Further research is necessary to improve the overall convective combustion model to better capture the material response and regression rate. This includes further experimental data at the small-scale that can include visual progression of a flame front within the *M1* bed while utilizing vents similar to large-scale experiments. Coupling the development of high fidelity CFD, FE structural analysis, and small-scale experiments will allow for a better understanding of the combustion environment and can aid in safety specifications for convective combustion events.

Acknowledgements

Funding: Support for this work has been provided by Josephine Covino at the Department of Defense Explosives Safety Board (DDESB). The authors would also like to thank Cynthia Romo and Alice Atwood for their continued support through the modeling process and provided valuable experimental data.

References

- [1] Cynthia Romo, Alice Atwood, and Josephine Covino. Sub-scale convective combustion of *m1* propellant. *JANNAF Proceedings*, 2017.
- [2] B. T. Bojko and P. E. DesJardin. On the development and application of a droplet flamelet-generated manifold for use in two-phase turbulent combustion simulations. *Comb. and Flame*, 183:50–65, 2017.
- [3] S.B. Pope. *Turbulent Flows*. Cambridge University Press, Cambridge, UK, 2000.
- [4] T. Poinso and Veynante D. *Theoretical and Numerical Combustion*. R.T. Edwards, Inc., Flourtown, PA, USA, 2005.
- [5] M.-S. Liou. A sequel to AUSM, part ii: AUSM+UP for all speeds. *J. Comput. Phys.*, 214(1):137 – 70, 2006.
- [6] Y. Li. Wavenumber-extended high-order upwind-biased finite-difference schemes for convective scalar transport. *J. Comput. Phys.*, 133:235–255, 1997.
- [7] J. A. Sethian and S. J. Osher. The design of algorithms for hypersurfaces moving with curvature-dependent speed, 1989. Notes on Numerical Fluid Mechanics, Volume 24.
- [8] Aubrey Farmer, Kevin P. Ford, Josephine Covino, Thomas L. Boggs, and Alice I. Atwood. Combustion of hazard division 1.3 *m1* gun propellant in a reinforced concrete structure. Technical report, TM8742, Naval Air Warfare Center Weapons Division, 2015.